Supporting Information

Role of Water in Proton-Coupled Electron Transfer between Tyrosine and Cysteine in Ribonucleotide Reductase

Jiayun Zhong,[1] Clorice R. Reinhardt,[2] and Sharon Hammes-Schiffer[1*]

[1]Department of Chemistry, Yale University, 225 Prospect Street, New Haven, Connecticut 06520, United States

[2]Department of Molecular Biophysics and Biochemistry, Yale University, 225 Prospect Street, New Haven, Connecticut 06520, United States

[*]Corresponding author email: sharon.hammes-schiffer@yale.edu

Table of Contents

System Setup	3
Equilibration	3
QM/MM Free Energy Simulations	4
Benchmarking QM Level of Theory	5
Further Analysis of QM/MM Strings	5
Figures	7
Tables	16
References	20

System Setup

The protocols for the system preparation and molecular dynamics (MD) simulations were adapted from our previous study of *E. coli* ribonucleotide reductase (RNR).[1] The partial charges for the diiron center and the tyrosine radical were obtained from this previous work.[1] All simulations started with the cryo-EM structure of the *E.coli* RNR $\alpha_2\beta_2$ complex (PDB ID: 6W4X).[2] Hydrogen atoms were added using H++ at pH 7.[3] The protein was immersed in TIP3P water[4] and neutralized with Na^+, followed by addition of Na^+ and Cl^- ions to adjust the salt concentration to be ~150 mM.

Equilibration

The equilibration procedure entailed energy minimizations and MD using the AMBER18 software package.[5] The ff14SB forcefield[6] and TIP3P water model were used for all molecular mechanical (MM) simulations in this work. The electrostatic interactions were described using the particle mesh Ewald method[7] with a cutoff distance of 10 Å. The NVT MD simulations used a Langevin thermostat with a 2 ps^{-1} collision frequency, and the NPT MD simulations used a Berendson barostat.[8] All MD simulations in this work used a time step of 1 fs. The equilibration protocol was as follows:

1. Minimization of the solvent and ions for 5000 steps using the steepest descent (SD) algorithm. Harmonic restraints with force constants of 500 kcal/(mol *$Å^2$) were applied to the protein atoms.
2. NVT MD of the solvent and ions at 300 K for 500 ps using the same restraint on the protein atoms as the first minimization step.
3. NPT MD of the solvent and ions at 300 K and 1 atm for 1 ns with 200 kcal/(mol *$Å^2$) harmonic restraints on the protein atoms.
4. 2000 steps of minimization of the protein with SD and 3000 steps of minimization using the conjugate gradient (CG) algorithm with 100 kcal/(mol *$Å^2$) harmonic restraints on the non-hydrogen atoms of the protein.
5. Same minimization of the protein as step 4 but with 100 kcal/(mol *$Å^2$) harmonic restraints on the backbone atoms of the protein.
6. Same minimization on the protein as step 4 but with 50 kcal/(mol *$Å^2$) harmonic restraints on the backbone atoms of the protein.
7. Same minimization on the protein as step 4 but with 10 kcal/(mol *$Å^2$) harmonic restraints on the backbone atoms of the protein.
8. Minimization of the protein for 2500 steps with SD and 2500 steps with CG without any restraints.
9. NPT heating of the entire system from 0 K to 300 K at 1 atm for 360 ps. For each step, the temperature was increased 50 K over 10 ps followed by an additional 50 ps equilibration at each resulting temperature.
10. NPT MD equilibration of the system at 300 K and 1 atm for 20 ns.
11. NVT MD equilibration of the system at 300 K for 20 ns.

QM/MM Free Energy Simulations

The procedure for the quantum mechanical/molecular mechanical (QM/MM) finite temperature string method with umbrella sampling was adapted from our work studying the PCET reaction between Y730 and Y731 in RNR.[9] The MM forcefield was the same as that described above for the equilibration. The QM region was described with density functional theory (DFT) using the ωB97X-D functional[10-13] and the 6-31+G** basis set.[11-13] Our benchmarking of this level of theory against *ab initio* multireference calculations is described below. The QM/MM interface was treated with hydrogen link atoms.[14] The SCF convergence criteria for the DFT calculations was 10^{-6}. All nonbonded interactions were included without any cut-off by setting the cut-off distance to 999 Å for the QM/MM simulations.

Three or four reaction coordinates were used for the QM/MM finite temperature string simulations (Figure S1). All of the string simulations used the reaction coordinates R1, R2, and R3, corresponding to the distance between the C439 sulfur and the transferring hydrogen, the distance between the Y730 oxygen and the transferring hydrogen, and the distance between this oxygen and sulfur, respectively. In some strings, a fourth reaction coordinate (R4) corresponding to the distance between a nearby water oxygen and the transferring hydrogen was also used.

The QM/MM MD string simulations with umbrella sampling were started from several different equilibrated configurations corresponding to flipped Y731 or stacked Y731 with either fully formed or slightly disrupted π-π stacking interactions. To generate the reactant and product, a proton was removed from either Y730 or C439 in the selected initial configuration. Water and ions further than 5 Å from the RNR complex except those within 18 Å of Y730 in the α (or α′) subunit were removed to decrease the computational cost. For the reactant and product, the QM region was optimized in the field of the frozen MM region with 200 steps of a hybrid of conjugate gradient and steepest descent algorithms. An approximate transition state structure was obtained by placing the transferring proton at the midpoint between Y730:OH and C439:SH, followed by 200 steps of energy minimization with harmonic restraints using force constants of 200 kcal/(mol *Å^2) applied to the reaction coordinates. Subsequently, an initial string was generated by quadratic interpolation of the QM atom coordinates corresponding to the reactant, approximate transition state, and product. This initial string was divided into 20 evenly spaced images for each system. Each image was equilibrated on the QM/MM potential energy surface by performing 10 ps of MD for the MM region with the atoms in the QM region frozen, followed by 100 fs MD for the full system with harmonic restraints applied to the reaction coordinates. For the string with stacked Y731 and a QM water, the full system was equilibrated for another 100 fs. After this initial equilibration, the iterative procedure for the finite temperature string method with umbrella sampling was started. Prior to each iteration, the harmonic restraints on the reaction coordinates for each image were determined by the average values of the reaction coordinates over the previous iteration, and the images were redistributed to be placed evenly along the string interpolating these values of the reaction coordinates. Each iteration entailed 100 fs of QM/MM MD for each image. The force constants for the harmonic restraints on the reaction coordinates were typically 100 kcal/(mol *Å^2), although this value was increased to 200 kcal/(mol *Å^2) for certain images (Table S1).

The strings were considered to be converged if they satisfied two main convergence criteria. The first convergence criterion is that the root-mean-square deviation (RMSD) between the reaction coordinates in the last iteration and the average values from the previous five iterations is less than 0.1 Å. The second convergence criterion is that the change in the free energy barrier over the last five iterations is less than 1 kcal/mol, and the overall free energy profiles are similar (Figure S10). The minimum free energy path (MFEP) was generated from the final iteration of the converged string, and the multidimensional free energy surface was generated using the data from all iterations using the weighted histogram analysis method (WHAM).[15-16] The bin size was 0.1 Å and the convergence criterion was 0.001 for the WHAM procedure. The standard deviations of 100 bootstrapped[15, 17] free energy profiles using the last iteration are shown as the error bars on the free energy profiles along the MFEPs (Figure S11).

Benchmarking QM Level of Theory

Our previous work established the suitability of the ωB97X-D functional[10-13] and the 6-31+G** basis set[11-13] by benchmarking against energies obtained with the complete active space self-consistent field with second-order perturbative corrections (CASSCF+NEVPT2) method. Specifically, proton potential energy curves were computed for the PCET reaction between Y731 and Y730 in the gas phase. We conducted a similar procedure to validate this functional for the PCET reaction between C439 and Y730 in the gas phase. For these calculations, we used the C439 and Y730 residues from the α chain of the cryo-EM structure[2] after adding and optimizing hydrogen atoms. Keeping all other nuclei fixed, we optimized the transferring hydrogen atom on C439 and Y730, corresponding to the reactant and product, respectively, with DFT, using the ωB97XD functional with the 6-31+G** basis set in the gas phase using the Gaussian 16 software package.[18] The coordinates for these two structures are given in Table S3. The proton transfer coordinate axis was defined to be along the line connecting the two optimized hydrogen positions, and the proton was positioned at twenty evenly spaced positions along this axis. We computed the energies at these proton coordinates using DFT with the following functionals: ωB97X–D and B3LYP [19-20] with the D3(BJ) dispersion correction.[21-22] We also computed these energies with the CASSCF+NEVPT2 method using PySCF[23] with an (11e, 10o) active space chosen by the atomic valence active space (AVAS) technique[24] embedded in the PiOS algorithm[25] and the 6-31+G** basis set. A comparison of these calculations is provided in Figure S2.

Further Analysis of QM/MM Strings

In this section, we provide a more detailed analysis of the three strings with Y731 and Y730 in the stacked conformation. In the first string, a water molecule introduced in the region near Y730 and C439 disrupted the stacking interaction and caused E623 and Q349 to move apart (Figure S3). In this string, Y731, Y730, C439, and Q349 were included in the QM region. As shown in Figure S6B the molecular mechanical water molecule remained near Y730 (~4.0 Å O-O distance) during the entire PCET reaction, forming a hydrogen bond with the Y730 hydroxyl group in the product state, similar to the behavior of the string with flipped Y731 and the same QM region

(Figure S4). The reaction free energy and free energy barriers (1 kcal/mol and 18 kcal/mol, respectively) are also very similar between these two strings.

In the second string for the stacked conformation, no water molecules were observed within ~6.0 Å (O-O distance) of Y730, and a stable stacking interaction between Y731 and Y730 was maintained for the entire MFEP. In this string, E623 was also included in the QM region and was found to hydrogen bond to the Y730 hydroxyl group in the product state, leading to a more exoergic reaction (–5 kcal/mol) but a similar free energy barrier (20 kcal/mol). This string illustrates that the electronic polarization of E623 is important for an accurate description of the hydrogen-bonding interaction that stabilizes the product.

In the third string for the stacked conformation, a water molecule was restrained to remain close to Y730 (~3.0 Å O-O distance) in the initial string. This string included Q349, E623, and this water molecule in the QM region, and the fourth reaction coordinate defined as the distance between the water oxygen and the transferring hydrogen was used. As the string evolved, this water moved away from Y730 in the reactant, with the distance between the water oxygen atom and the transferring hydrogen greater than ~4.0 Å. In the product, this water formed a weak hydrogen bond with Y730 (~3.3 Å O-O distance, angle of 109°), and E623 formed a stronger hydrogen bond with Y730 (~2.6 Å O-O distance, angle of 135°). The observation that E623 forms a hydrogen bond with Y730 in the product is consistent with the observation of this hydrogen bond for the string with stacked Y731 and Q349 and E623 in the QM region (Table 1, Fig S7, Table S2).

To investigate this PCET reaction in the post-turnover state, we also propagated two strings in the α′ subunit with flipped Y731. The MFEPs and free energy surfaces are qualitatively similar in the α and α′ subunits (Table 1). The impact of treating the water quantum mechanically on radical transfer from Y730 to C439, namely making the reaction exoergic and lowering the free energy barrier, is even more pronounced for the post-turnover state. The quantitative differences are most likely due to structural differences. Nevertheless, the reproducibility of the qualitative impact of the water molecule on the thermodynamics of this PCET reaction provides further validation for this phenomenon.

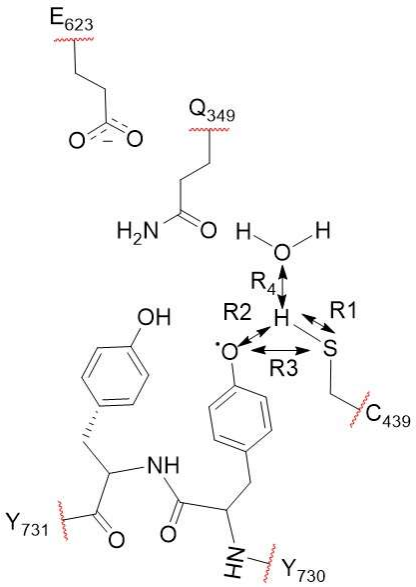

Figure S1. QM regions and reaction coordinates used in the QM/MM string simulations. All strings included Y731, Y730, and C439 in the QM region and have at least three reaction coordinates corresponding to the distance between the C439 sulfur and the transferring hydrogen (R1), the distance between the Y730 oxygen and the transferring hydrogen (R2), and the distance between this oxygen and sulfur (R3). The strings in the α subunit also included Q349 in the QM region, and some of these strings included E623 or a water molecule in the QM region. The atoms included in the QM region for these various residues are indicated by the red boundaries. A fourth reaction coordinate between the water oxygen and the transferring hydrogen (R4) was added for some strings with water in the QM region.

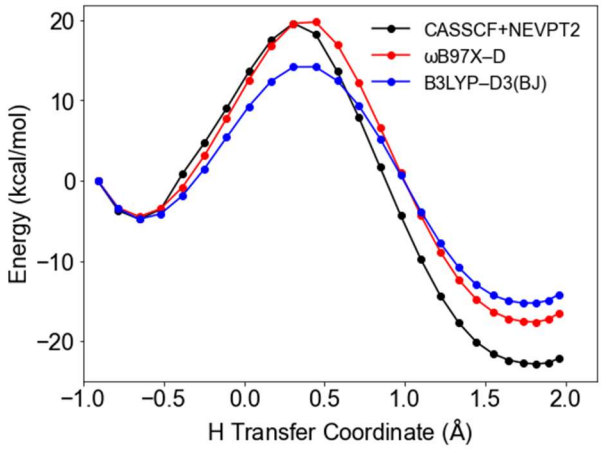

Figure S2. Ground state potential energies corresponding to PCET between C439 and Y730 along the hydrogen transfer coordinate calculated with the CASSCF+NEVPT2 method and with DFT using the ωB97X–D and B3LYP–D3(BJ) functionals.

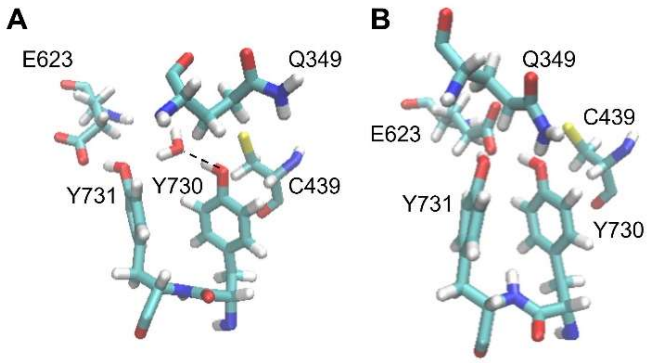

Figure S3. Comparison of product configurations with (A) and without (B) water near the QM region, illustrating disrupted or fully formed π-π stacking interactions between Y730 and Y731, respectively. Water is able to form a hydrogen bond (dashed line) with Y730 in the product when the Y730 and Y731 are separated and tilted in a manner that disrupts their stacking interaction. This water molecule stays within ~4 Å of the Y730 oxygen atom during the PCET reaction. Moreover, E623 is further away from Y730, with its oxygen atom closer to the oxygen atom of Y731, and Q349 is reoriented with its nitrogen atom pointing away from the Y730 oxygen. These configurations were obtained from the final iteration of the string with stacked Y731, Y730, C439, and Q349 in the QM region for part A and the string with the addition of E623 to the QM region for part B.

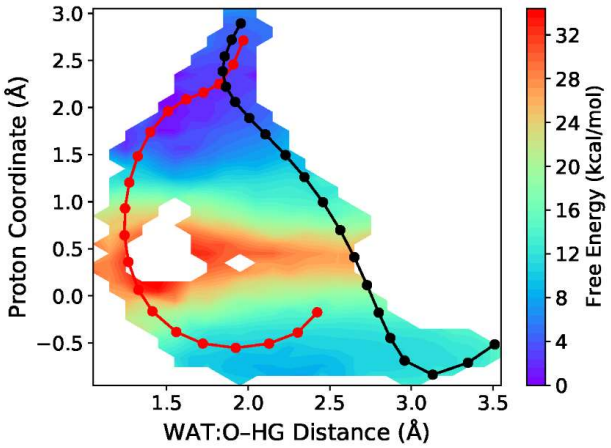

Figure S4. Two-dimensional free energy surfaces for the PCET reaction associated with radical transfer from Y730α to C439α for the string with flipped Y731, Y730, C439, Q349, and water in the QM region and using four reaction coordinates. The *y*-axis is the hydrogen transfer coordinate, defined as the difference between the C439 sulfur-hydrogen and Y730 oxygen-hydrogen distances, and the *x*-axis the distance between the water oxygen and the transferring hydrogen. The red curve is the initial string after QM/MM equilibration of the images, and the black curve corresponds to the MFEP from the converged string. The initial string was obtained by forcing the proton to transfer to water, generating H_3O^+, as it transfers between C439 and Y730. The remainder of the system was relaxed around these structures, and each image along this initial string was equilibrated with the reaction coordinates harmonically restrained. Comparison between the red and black curves shows that the string evolved away from this initial string so that the proton did not covalently bind to the water molecule and instead transferred directly from C439 to Y730. The data from the first iteration of the string was not included to ensure adequate equilibration; in this case, the free energy barrier and reaction free energy were 15.4 kcal/mol and –8.6 kcal/mol, respectively. A different depiction of this string is provided in Figure 2A of the main paper.

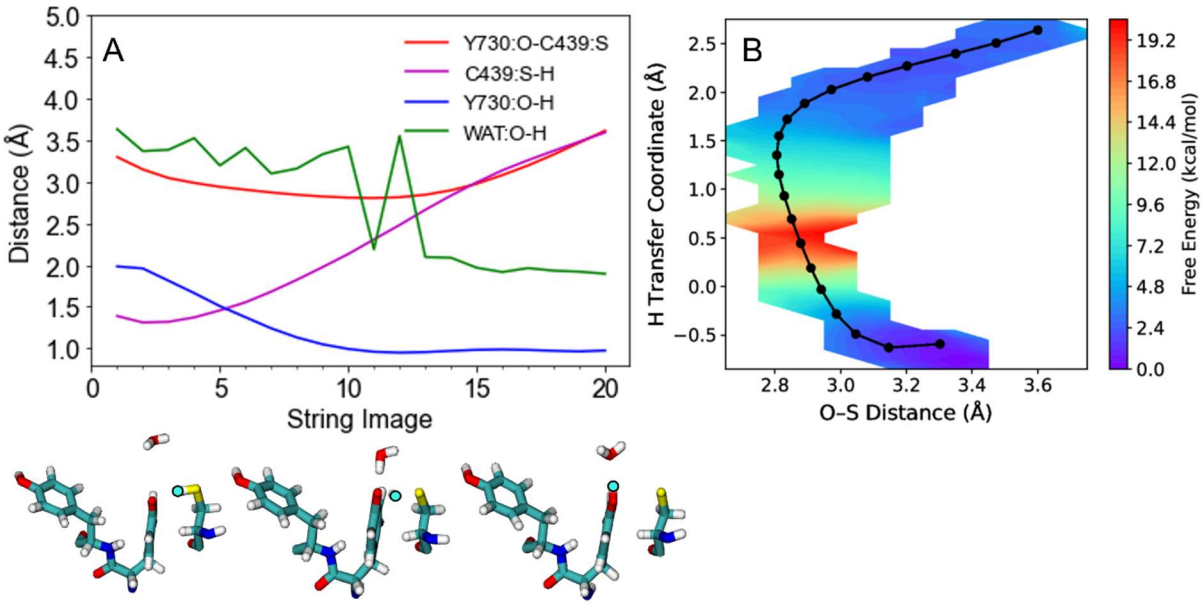

Figure S5. (A) Average distances between the Y730 oxygen and C439 sulfur, as well as between the transferring hydrogen and the C439 sulfur, Y730 oxygen, and water oxygen, and (B) two-dimensional free energy surfaces and MFEP (black curve) for the PCET reaction associated with radical transfer from Y730α to C439α for the string with flipped Y731, Y730, C439, and Q349 in the QM region and a nearby water treated molecular mechanically. Although this water fluctuates more than the water treated quantum mechanically (Figures 2A and 3A), they both exhibit the similar trend that water moves closer to the transferring proton as the radical transfers from Y730 to C439. In part A, the average distances were obtained from the final iteration of the converged string. In part B, the data from the first three iterations of the string was not included to ensure adequate equilibration; in this case, the free energy barrier and reaction free energy were 17.4 kcal/mol and 1.6 kcal/mol, respectively.

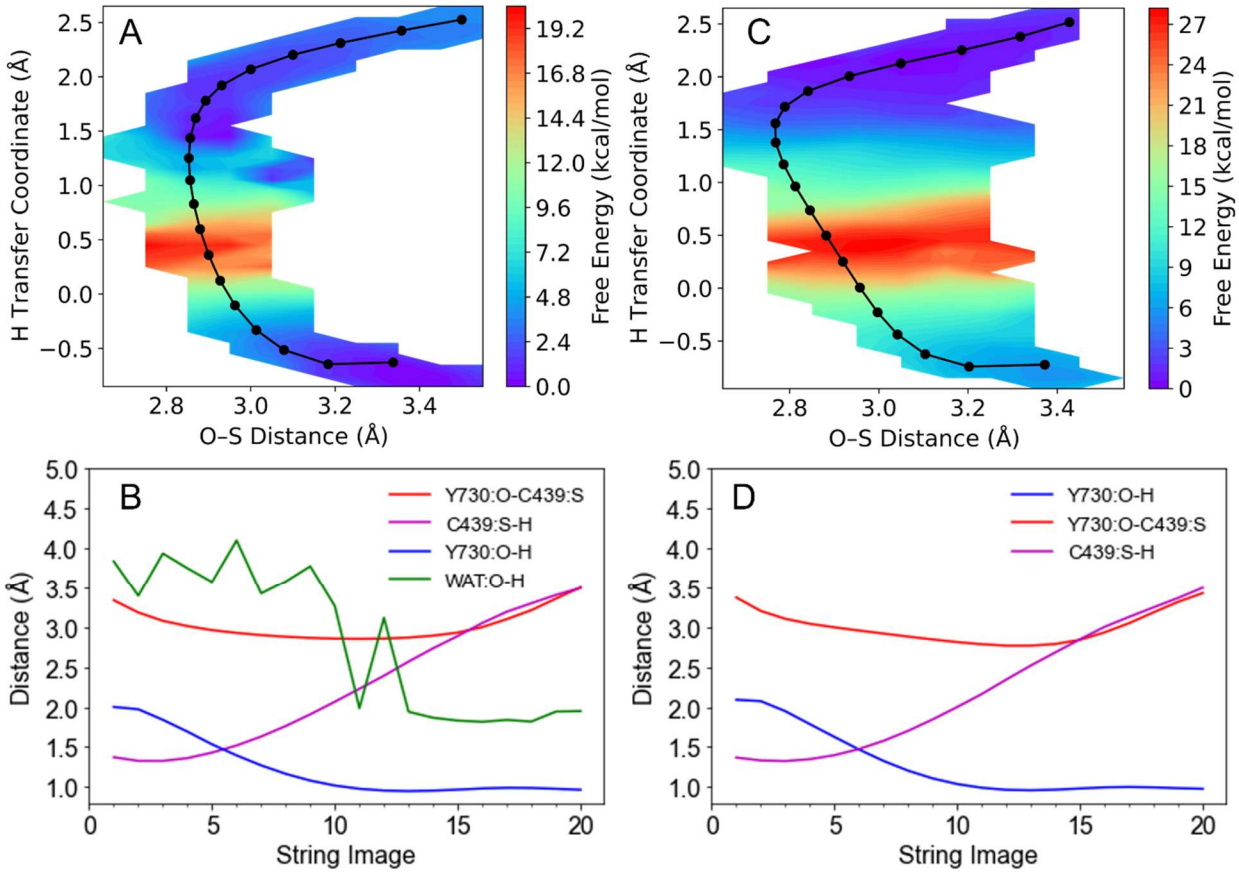

Figure S6. Two-dimensional free energy surfaces and average distances for the PCET reaction associated with radical transfer from Y730α to C439α for the strings with stacked Y731 and (A, B) Q349 in the QM region and water remaining within ~4.0 Å of Y730, disrupting the stacking interaction or (C, D) Q349 and E623 in the QM region. Both strings used three reaction coordinates. The stacking interaction is disrupted in part A but is fully formed in part B. The average distances were obtained from the final iterations of the converged strings.

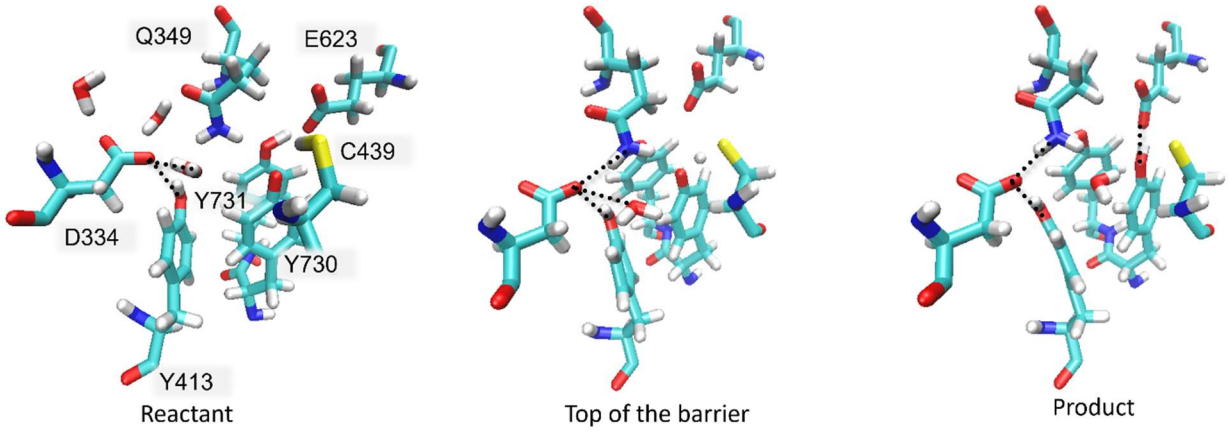

Figure S7. Representative configurations from the final iteration of the converged string with stacked Y731, Y730, C439, Q349, E623, and water in the QM region. Although water does not interact strongly with Y730 in this string, the reaction barrier and reaction free energy were lowered compared to the string in which water did not remain close to Y730 (Table 1), most likely due to the enhanced hydrogen-bonding interactions among the water, Q349, D334, and Y413. The hydrogen-bonding interactions are shown with dotted black lines. Note that D334 and Y413 were considered to be in the vicinity of the key water in previous DFT calculations.[26]

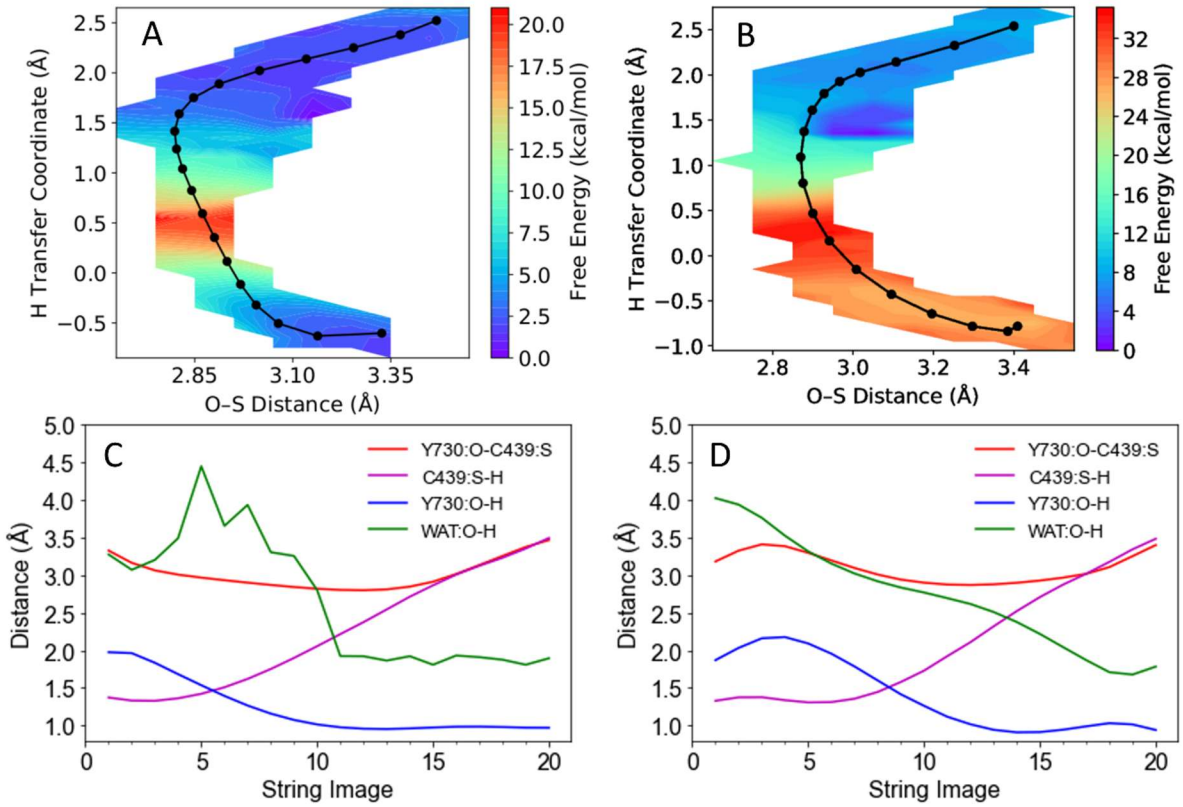

Figure S8. Two-dimensional free energy surfaces and average distances for the PCET reaction associated with radical transfer from Y730α′ to C439α′ for the string with flipped Y731 and (A, C) water in the MM region and (B,D) water in the QM region. The string in parts A and C used three reaction coordinates, and the string in parts B and D used four reaction coordinates. The average distances were obtained from the final iterations of the converged strings. In parts A and B, the data from the first three iterations of the strings was not included to ensure adequate equilibration; in this case, the free energy barrier and reaction free energy were 15.4 kcal/mol and –0.1 kcal/mol, respectively, in parts A, C and 10.0 kcal/mol and –20.8 kcal/mol, respectively, in parts B, D. Sampling in this subunit is considerably more challenging.

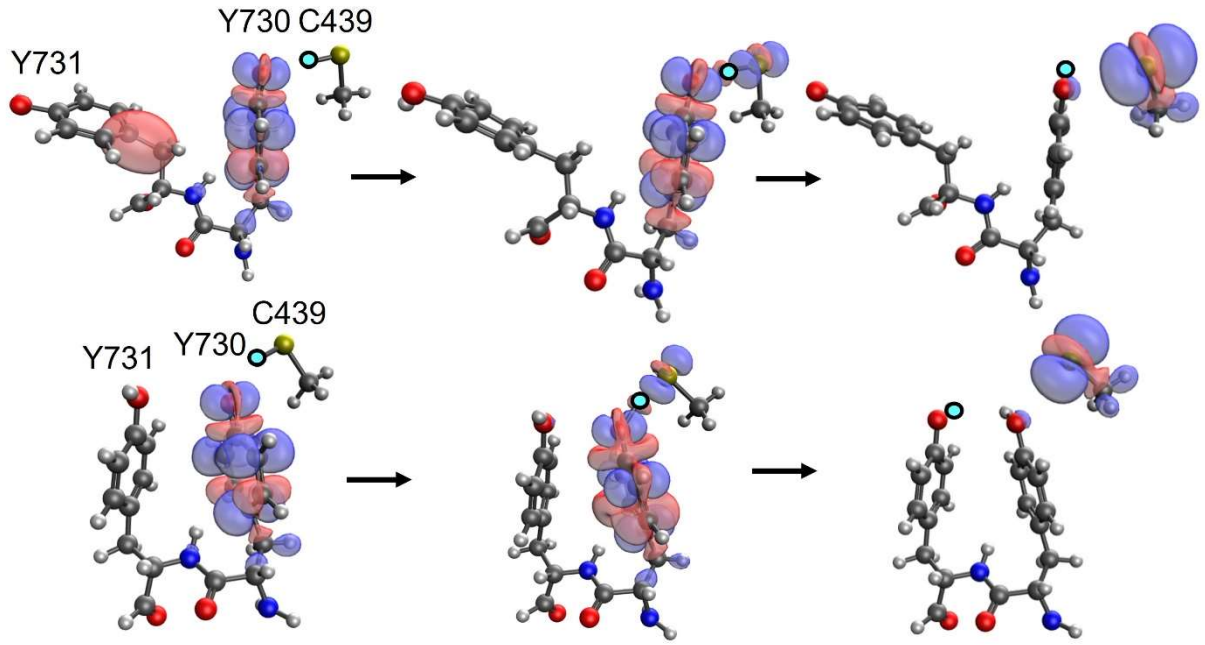

Figure S9. Spin densities computed for representative configurations along the MFEP from the converged strings for flipped (top) and stacked (bottom) Y731. The configurations correspond approximately to the reactant (left), top of the barrier (middle), and product (right). The spin density calculations were performed with DFT/ωB97X-D/6-31+G** in the gas phase, and the analogous *ab initio* multireference results are provided in the main text (Figure 5). The transferring proton is shown in bright cyan. A Mulliken spin population analysis indicates that the spin density on Y731 for the reactant of the flipped Y731 conformation (shown in red) is negligible (≤ 1%).

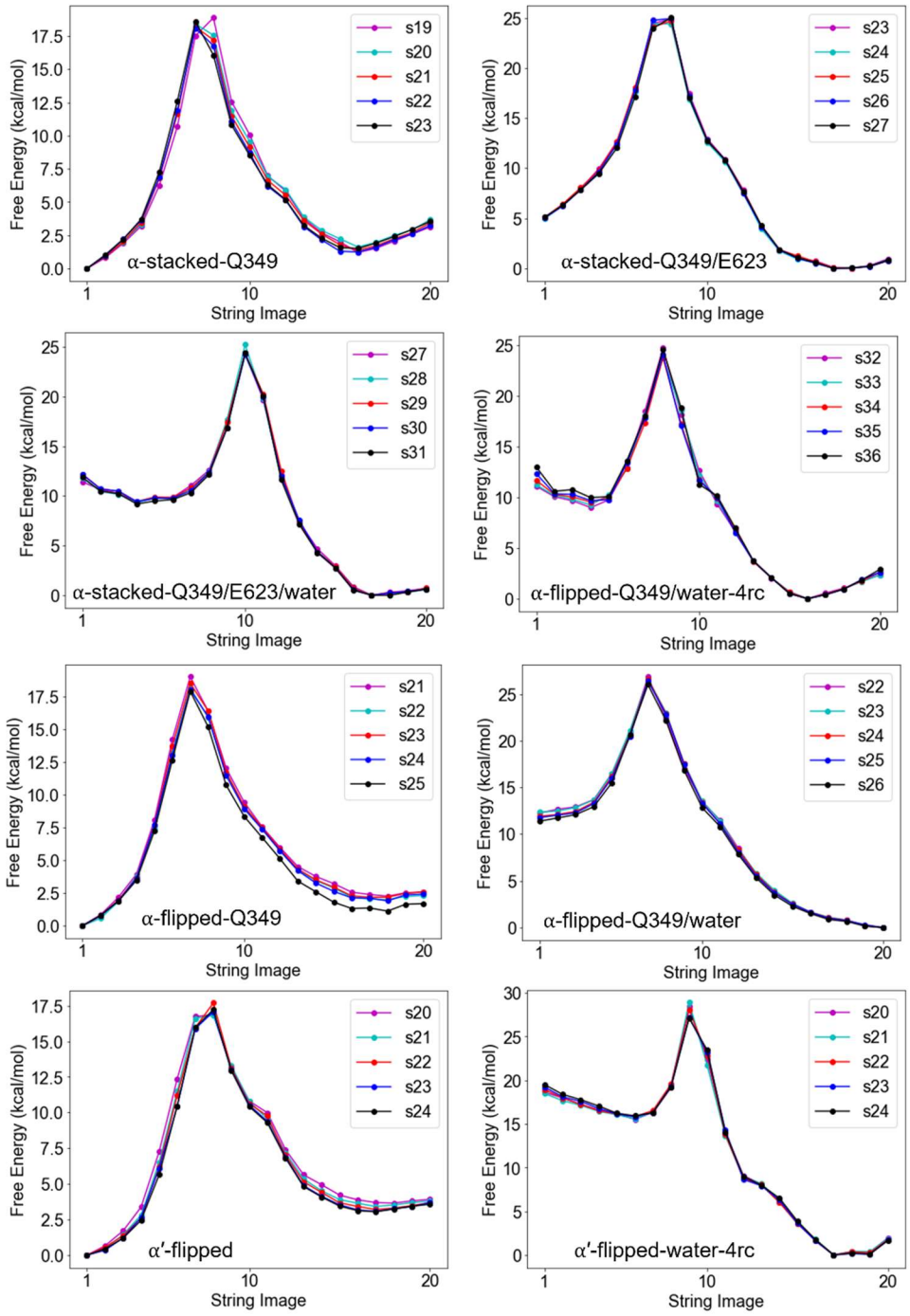

Figure S10. Free energy profiles along the MFEPs for the last five iterations of all strings labeled by their subunits, Y731 conformation, and the QM region residues in addition to Y730, Y731, and C439.

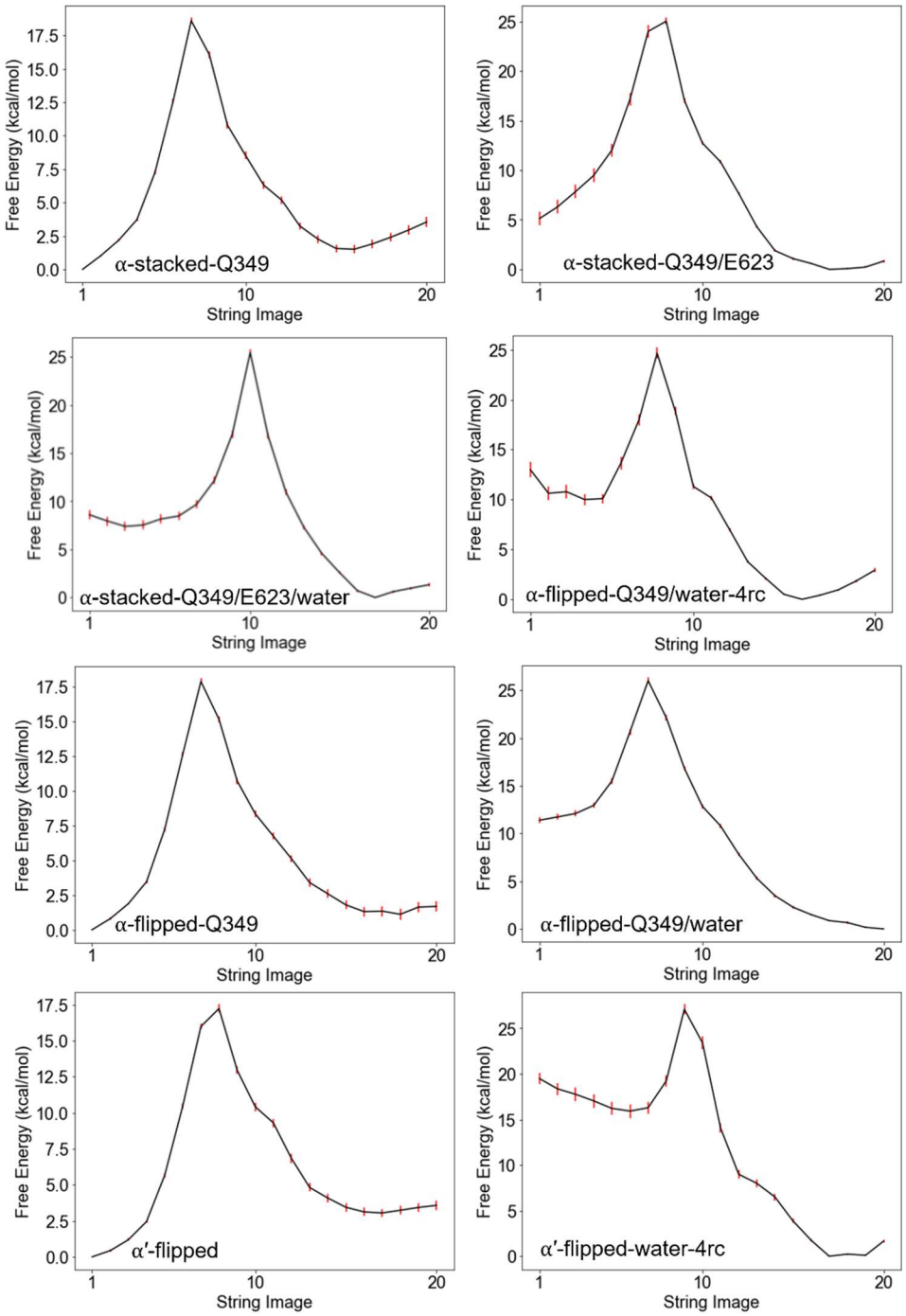

Figure S11. Free energy profiles with error bars from bootstrapping along the MFEPs for the last iterations of all strings labeled by their subunits, Y731 conformation, and the QM region residues in addition to Y730, Y731, and C439.

Table S1. Images with 200 kcal/(mol *Å^2) Harmonic Restraints on R1 and R2 during QM/MM String Simulations

Systems	QM Region[a]	Iteration	Image Number
α-Stacked[b]	Q349	1-5	9-11
α-Stacked	Q349, E623	1-16, 25-27	7-9
α-Stacked[c]	Q349, E623, H_2O	1-2	1-20
		3-31	9-11
α-Flipped	Q349	1,3	10-12
		2	7-9
		4	10
		5	7-10
α-Flipped	Q349, H_2O	2	7-8
		4-7	7-9
		8-10	6-9
		11-12,14-15,19-20	6-7
α-Flipped[c]	Q349, H_2O	9-13	9-10
		14-15	7-10
		17-18, 20, 22	8-10
α′-Flipped		2-7,10,12-13,15-16	7-9
α′-Flipped[c]	H_2O	0	16-17
		1	12-15
		2	11
		3	10
		4	9-11
		6,8	9
		9-17	9-10

[a] All QM regions include Y730, Y731, and C439.
[b] Y731 and Y730 are not completely stacked (Figure S3).
[c] A fourth harmonic restraint was applied to WAT:O-H (Figure S1).

Table S2. Analysis of QM versus MM Treatment of Key Water[a]

QM region residues including QM water[b]	QM region residues plus two closest MM waters[c]	QM region residues plus entire MM region[d]
0.4	–5.1	–9.9

[a] Average energies in kcal/mol were calculated for the 100 configurations from the images corresponding to the reactant and product in the last iteration of the converged string for radical transfer from Y730α to C439α with flipped Y731 and the QM region composed of Y731, Y730, C439, Q349, and water and four reaction coordinates. These energies were computed with the QM region water treated either quantum mechanically or molecular mechanically for this analysis. The energy values given in this table correspond to the difference between the QM and MM treatments of this water: $\Delta\Delta E = \Delta E$(QM water) – ΔE(MM water), where each ΔE is the difference between the average energy for the product image and the average energy for the reactant image. These calculations were performed with different environments as indicated by the column headings. Each energy is computed as the energy of the QM region in the field of the point charges in the MM environment using electrostatic embedding.

[b] These energies were calculated for only the QM region, including the QM water. The QM and MM treatments of this water molecule led to similar energetics. Similarly, when gas phase systems composed of a tyrosyl radical and water or a tyrosine and water, corresponding to the reactant and product, respectively, were each optimized at the QM level, followed by single-point energy calculations for these geometries with the water treated either QM or MM, the analogous $\Delta\Delta E$ value was less than ~1 kcal/mol. These calculations illustrate that the MM treatment of the water does not significantly alter the relative energetics of the tyrosine-water and tyrosyl radical-water systems.

[c] These energies were calculated for the QM region, including the QM water, plus the two closest MM waters. The larger $\Delta\Delta E$ indicates that the polarization of the QM water by the charges of the two MM waters significantly impacts the energies. When this water is treated molecular mechanically with fixed charges, this polarization effect is absent.

[d] These energies were calculated for the QM region, including the QM water, plus all MM atoms of the system used in the string calculations. The larger $\Delta\Delta E$ indicates that the polarization of the QM water by the MM charges significantly impacts the energies. When this water is treated molecular mechanically with fixed charges, this polarization effect is absent.

Table S3. Hydrogen Bond Analysis for Y730 Oxygen in QM/MM Strings[a]

System	Interacting Entity	O–O Distance (Å)	O-H-O Angle (°)	O–H Distance (Å)
Stacked, Top of Barrier[b]	E623			3.4
Stacked, Product[b]	E623	2.8	169	
Stacked, Top of Barrier[c]	E623			3.7
Stacked, Product[c]	E623	2.6	135	
Stacked, Product[c]	H_2O	3.3	109	
Flipped, Reactant[d]	H_2O	3.2	125	
Flipped, Top of Barrier[d]	H_2O			2.7
Flipped, Product[d]	H_2O	2.8	157	

[a] Average distances and angles are determined for the images corresponding to the reactant minimum, product minimum, and top of the barrier in the MFEP for the last iteration of the converged string. Note that these are direct averages for the specified image without accounting for the biasing potential, although unbiasing does not significantly alter the values. The O–O distance and O-H-O angle refer to the hydrogen bond donor-acceptor distance and angle, respectively, for the hydrogen bond between E623 or H_2O and the Y730 hydroxyl group. The O–H distance refers to the distance between the E623 or H_2O oxygen and the transferring hydrogen when the hydrogen is midway (i.e., at the top of the barrier).

[b] These values were obtained from the string for radical transfer from Y730α to C439α with stacked Y731 and the QM region composed of Y731, Y730, C439, Q349, and E623 with no water near Y730. This string used three reaction coordinates. No persistent hydrogen bond was observed between E623 and Y730 in the reactant, and the electrostatic interaction between the E623 oxygen and the transferring hydrogen is very weak at the top of the barrier. The hydrogen bond (O-O distance $\leq$ 3.0 Å and O-H-O angle $\geq$ 135°) between E623 and Y730 was present in the product for all frames in the last iteration.

[c] These values were obtained from the string for radical transfer from Y730α to C439α with stacked Y731 and the QM region composed of Y731, Y730, C439, Q349, E623, and water on the Q349 side of Y730. This string used three reaction coordinates. No persistent hydrogen bond was observed between E623 and Y730 in the reactant, and the electrostatic interaction between the E623 oxygen and the transferring hydrogen is very weak at the top of the barrier. The hydrogen bond (O-O distance $\leq$ 3.0 Å and O-H-O angle $\geq$ 135°) between E623 and Y730 was present in the product for all frames in the last iteration. A weak hydrogen bond with water as the donor and Y730 as the acceptor was also present in the product.

[d] These values were obtained from the string for radical transfer from Y730α to C439α with flipped Y731 and the QM region composed of Y731, Y730, C439, Q349, and water with four reaction coordinates. Note that water acts as a weak hydrogen bond donor in the reactant and as a much stronger hydrogen bond acceptor in the product. The electrostatic interaction between the water and the transferring hydrogen is also significant at the top of the barrier. The hydrogen bond (O-O distance $\leq$ 3.0 Å and O-H-O angle $\geq$ 135°) between E623 and Y730 was present in the product for all frames in the last iteration.

Table S4. Reactant Structure of Y730/C439 Gas Phase Model System with Fixed Nuclei of All Atoms except the Transferring H Atom Used For Benchmarking

Atom	**X**	**Y**	**Z**
N	-3.975359	1.926407	1.257277
C	-2.937148	1.317516	0.439039
C	-1.941009	2.331507	-0.112994
O	-1.276561	2.044482	-1.11282
C	-3.574885	0.537094	-0.711118
S	-4.063628	-1.149469	-0.296641
N	5.019129	1.522029	-0.73967
C	4.002297	0.6893	-0.085282
C	4.584206	-0.46398	0.732548
O	4.544003	-0.439791	1.963493
C	3.035491	0.169541	-1.151093
C	1.770833	-0.444638	-0.615336
C	1.199307	0.010821	0.556659
C	1.150043	-1.487596	-1.285405
C	0.044431	-0.551124	1.048164
C	-0.007648	-2.051999	-0.808259
C	-0.555474	-1.583607	0.363716
O	-1.710427	-2.146408	0.855932
H	-3.601567	2.279568	2.132861
H	-4.66873	1.226149	1.502167
H	-2.307112	0.611919	1.006766
H	-1.810413	3.295008	0.413603
H	-4.474961	1.07038	-1.031226
H	-2.88846	0.508291	-1.556978
H	5.594503	1.99945	-0.054863
H	4.574533	2.222449	-1.321592
H	3.445766	1.278184	0.653745
H	5.043306	-1.308973	0.186356
H	3.558199	-0.538357	-1.804787
H	2.754341	1.017809	-1.790669
H	1.651725	0.818917	1.118195
H	1.590492	-1.865974	-2.204307
H	-0.392274	-0.216951	1.983006
H	-0.493609	-2.871231	-1.327559
H[a]	-2.942873	-1.777452	-0.658357
H[b]	**-1.95434**	**-2.908716**	**0.276334**

[a]The optimized position of the proton at the donor S atom.
[b]The optimized position of the proton at the acceptor O atom. These two proton positions were used to generate the one-dimensional proton coordinate axis for benchmarking.

References

(1) Reinhardt, C. R.; Li, P.; Kang, G.; Stubbe, J.; Drennan, C. L.; Hammes-Schiffer, S., Conformational Motions and Water Networks at the α/β Interface in E. coli Ribonucleotide Reductase. *J. Am. Chem. Soc.* **2020,** *142*, 13768-13778.
(2) Kang, G.; Taguchi, A. T.; Stubbe, J.; Drennan, C. L., Structure of a trapped radical transfer pathway within a ribonucleotide reductase holocomplex. *Science* **2020,** *368*, 424-427.
(3) Gordon, J. C.; Myers, J. B.; Folta, T.; Shoja, V.; Heath, L. S.; Onufriev, A., H++: a server for estimating pKas and adding missing hydrogens to macromolecules *Nucleic Acids Res.* **2005,** *33*, W368-W371.
(4) Jorgensen, W. L. C., J.; Madura, J. D.; Impey, R. W.; Klein, M. L. , Comparison of simple potential functions for simulating liquid water. *J. Chem. Phys.* **1983,** *79*, 926-935.
(5) Salomon-Ferrer, R.; Götz, A. W.; Poole, D.; Le Grand, S.; Walker, R. C., Routine Microsecond Molecular Dynamics Simulations with AMBER on GPUs. 2. Explicit Solvent Particle Mesh Ewald. *J. Chem. Theory Comput.* **2013,** *9*, 3878-3888.
(6) Maier, J. A.; Martinez, C.; Kasavajhala, K.; Wickstrom, L.; Hauser, K. E.; Simmerling, C., ff14SB: Improving the Accuracy of Protein Side Chain and Backbone Parameters from ff99SB. *J. Chem. Theory Comput.* **2015,** *11*, 3696-3713.
(7) Darden, T.; York, D.; Pedersen, L., Particle mesh Ewald: An N·log(N) method for Ewald sums in large systems. *J. Chem. Phys.* **1993,** *98*, 10089-10092.
(8) Ryckaert, J.-P.; Ciccotti, G.; Berendsen, H. J., Numerical integration of the cartesian equations of motion of a system with constraints: molecular dynamics of n-alkanes. *J. Comp. Phys.* **1977,** *23*, 327-341.
(9) Reinhardt, C. R.; Sayfutyarova, E. R.; Zhong, J.; S., H.-S., Glutamate Mediates Proton-Coupled Electron Transfer Between Tyrosines 730 and 731 in Escherichia coli Ribonucleotide Reductase. *J. Am. Chem. Soc.* **2021,** *143*, 6054-6059.
(10) Chai, J.-D.; Head-Gordon, M., Long-range corrected hybrid density functionals with damped atom–atom dispersion corrections. *Phys. Chem. Chem. Phys.* **2008,** *10*, 6615-6620.
(11) Hehre, W. J.; Ditchfield, R.; Pople, J. A., Self-consistent molecular orbital methods. XII. Further extensions of Gaussian—type basis sets for use in molecular orbital studies of organic molecules. *J. Chem. Phys.* **1972,** *56*, 2257-2261.
(12) Clark, T.; Chandrasekhar, J.; Spitznagel, G. W.; Schleyer, P. V. R., Efficient diffuse function-augmented basis sets for anion calculations. III. The 3-21+G basis set for first-row elements, Li–F. *J. Comput. Chem.* **1983,** *4*, 294-301.
(13) Hariharan, P. C.; Pople, J. A., The influence of polarization functions on molecular orbital hydrogenation energies. *Theor. Chim. Acta.* **1973,** *28*, 213-222.
(14) Gotz, A. W.; Clark, M. A.; Walker, R. C., An extensible interface for QM/MM molecular dynamics simulations with AMBER. *J. Comput. Chem.* **2014,** *35*, 95-108.
(15) Grossfield, A. *WHAM: the weighted histogram analysis method.*, WHAM version 2.0.9.
(16) Souaille, M.; Roux, B. t., Extension to the weighted histogram analysis method: combining umbrella sampling with free energy calculations. *Comput. Phys. Commun.* **2001,** *135*, 40-57.
(17) Hub, J. S.; de Groot, B. L.; van der Spoel, D., g_wham—A Free Weighted Histogram Analysis Implementation Including Robust Error and Autocorrelation Estimates. *J. Chem. Theory Comput.* **2010,** *6*, 3713-3720.
(18) Frisch, M. J.; Trucks, G. W.; Schlegel, H. B.; Scuseria, G. E.; Robb, M. A.; Cheeseman, J. R.; Scalmani, G.; Barone, V.; Petersson, G. A.; Nakatsuji, H.; Li, X.; Caricato, M.; Marenich, A. V.; Bloino, J.; Janesko, B. G.; Gomperts, R.; Mennucci, B.; Hratchian, H. P.; Ortiz, J. V.; Izmaylov, A. F.; Sonnenberg, J. L.; Williams-Young, D.; Ding, F.; Lipparini, F.; Egidi, F.; Goings, J.; Peng, B.; Petrone, A.; Henderson, T.; Ranasinghe, D.; Zakrzewski, V. G.; Gao, J.; Rega, N.; Zheng, G.; Liang, W.; Hada, M.; Ehara, M.; Toyota, K.; Fukuda, R.; Hasegawa, J.; Ishida, M.; Nakajima, T.; Honda, Y.; Kitao, O.; Nakai, H.; Vreven, T.; Throssell, K.; J. A. Montgomery, J.; Peralta, J. E.; Ogliaro, F.; Bearpark, M. J.; Heyd, J. J.; Brothers, E. N.; Kudin, K. N.; Staroverov, V. N.; Keith, T. A.; Kobayashi, R.; Normand, J.;

Raghavachari, K.; Rendell, A. P.; Burant, J. C.; Iyengar, S. S.; Tomasi, J.; Cossi, M.; Millam, J. M.; Klene, M.; Adamo, C.; Cammi, R.; Ochterski, J. W.; Martin, R. L.; Morokuma, K.; Farkas, O.; Foresman, J. B.; Fox, D. J., Gaussian 16 Revision D.01. **2016**.
(19) Lee, C.; Yang, W.; Parr, R. G., Development of the Colle-Salvetti correlation-energy formula into a functional of the electron density. *Phys. Rev. B* **1988,** *37*, 785-789.
(20) Becke, A. D., Density-functional thermochemistry. III. The role of exact exchange. *J. Chem. Phys.* **1993,** *98*, 5648-5652.
(21) Grimme, S.; Ehrlich, S.; Goerigk, L., Effect of the damping function in dispersion corrected density functional theory. *J Comput Chem* **2011,** *32*, 1456-65.
(22) Grimme, S.; Antony, J.; Ehrlich, S.; Krieg, H., A consistent and accurate ab initio parametrization of density functional dispersion correction (DFT-D) for the 94 elements H-Pu. *J. Chem. Phys.* **2010,** *132*, 154104.
(23) Sun, Q.; Berkelbach, T. C.; Blunt, N. S.; Booth, G. H.; Guo, S.; Li, Z.; Liu, J.; McClain, J. D.; Sayfutyarova, E. R.; Sharma, S.; Wouters, S.; Chan, G. K.-L., PySCF: the Python-based simulations of chemistry framework. *WIREs: Comput. Mol. Sci.* **2018,** *8*.
(24) Sayfutyarova, E. R.; Sun, Q.; Chan, G. K.-L.; Knizia, G., Automatic construction of molecular active spaces from atomic valence orbitals. *J. Chem. Theory Comput.* **2017,** *13*, 4063–4078.
(25) Sayfutyarova, E. R.; Hammes-Schiffer, S., Constructing Molecular π-Orbital Active Spaces for Multireference Calculations of Conjugated Systems. *J. Chem. Theory Comput.* **2019,** *15*, 1679-1689.
(26) Argirević, T.; Riplinger, C.; Stubbe, J.; Neese, F.; Bennati, M., ENDOR Spectroscopy and DFT Calculations: Evidence for the Hydrogen-Bond Network Within α2 in the PCET of E. coli Ribonucleotide Reductase. *J. Am. Chem. Soc.* **2012,** *134*, 17661-17670.